



Universiteit
Leiden
The Netherlands

The Journal of cardiovascular computed tomography year in review: 2019

Choi, J.W.; Rosendael, A.R. van; Bax, A.M.; Hoogen, I.J. van den; Gianni, U.; Baskaran, L.; ... ; Al'Aref, S.J.

Citation

Choi, J. W., Rosendael, A. R. van, Bax, A. M., Hoogen, I. J. van den, Gianni, U., Baskaran, L., ... Al'Aref, S. J. (2020). The Journal of cardiovascular computed tomography year in review: 2019. *Journal Of Cardiovascular Computed Tomography*, 14(2), 107-117.
doi:10.1016/j.jcct.2020.01.003

Version: Publisher's Version

License: [Creative Commons CC BY 4.0 license](#)

Downloaded from: <https://hdl.handle.net/1887/3731141>

Note: To cite this publication please use the final published version (if applicable).



The Journal of Cardiovascular Computed Tomography year in review – 2019

Jeong W. Choi^a, Alexander R. van Rosendael^a, A. Maxim Bax^a, Inge J. van den Hoogen^a, Umberto Gianni^a, Lohendran Baskaran^{a,b}, Daniele Andreini^c, Carlo N. De Cecco^d, James Earls^e, Maros Ferencik^f, Harvey Hecht^g, Jonathon A. Leipsic^h, Pál Maurovich-Horvatⁱ, Edward Nicol^j, Gianluca Pontone^c, Subha Raman^k, Paul Schoenhagen^l, Armin Arbab-Zadeh^m, Andrew D. Choi^e, Gudrun Feuchtnerⁿ, Jonathan Weir-McCall^o, Kavitha Chinnaiyan^p, Seamus Whelton^m, James K. Min^q, Todd C. Villines^r, Subhi J. Al'Aref^{q,a,*}

^a Dalio Institute of Cardiovascular Imaging, Weill Cornell Medicine and New York-Presbyterian Hospital, New York, NY, USA

^b Department of Cardiovascular Medicine, National Heart Centre, Singapore

^c Centro Cardiologico Monzino, IRCCS, Milan, Italy

^d Division of Cardiothoracic Imaging, Nuclear Medicine and Molecular Imaging, Emory University, Atlanta, GA, USA

^e The George Washington University School of Medicine and Health Sciences, Washington, DC, USA

^f Knight Cardiovascular Institute, Oregon Health & Science University, Portland, OR, USA

^g Icahn School of Medicine at Mount Sinai, New York, NY, USA

^h Department of Medicine and Radiology, University of British Columbia, Vancouver, BC, Canada

ⁱ Medical Imaging Centre, Department of Radiology, Semmelweis University, Budapest, Hungary

^j Royal Brompton Hospital, London, UK

^k Ohio State University, Columbus, OH, USA

^l Cleveland Clinic, Cleveland, OH, USA

^m Johns Hopkins University School of Medicine, Baltimore, MD, USA

ⁿ Department of Internal Medicine III, Cardiology, Innsbruck Medical University, Innsbruck, Austria

^o School of Clinical Medicine, University of Cambridge, Cambridge, UK

^p Department of Cardiology, William Beaumont Hospital, Royal Oak, MI, USA

^q Cleerly Inc, New York, NY, USA

^r Division of Cardiovascular Medicine, University of Virginia Health System, Charlottesville, VA, USA

ABSTRACT

The purpose of this review is to summarize the work published by the Journal of Cardiovascular Computed Tomography (JCCT) for the year 2019, highlighting original research and new guidelines.

1. Introduction

In 1979, the Nobel Prize in Physics and Medicine was awarded to Sir Godfrey Newbold Hounsfield and Allan MacLeod Cormack for their discovery of computer assisted tomography.¹ Ever since then, the field of cardiac computed tomography (CCT) has continued to adapt and evolve in response to the inexorable progress in our understanding of cardiovascular disease. In this review, we highlight the year of the Journal of Cardiovascular Computed Tomography (JCCT) with respect to six broad categories: (1) coronary artery disease (CAD), (2) coronary physiology, (3) structural heart disease, (4) non-cardiac assessment on computed tomography (CT), (5) technical aspects of CCT, and (6)

technological advances.

With a record number of submissions, the year 2019 has been very busy for the JCCT (Table 1). It follows then, that the acceptance rate for research manuscripts was lower for 2019 at 20%, while in 2018 it was 33%. The following is a summary of the research insights of our community for the benefit of our readership. As this review was completed before the year's end, more recent work will be addressed in the next year in review.

2. Topic 1: Coronary artery disease

In the *January-February* issue, Deseive and colleagues presented data

* Corresponding author. Dalio Institute of Cardiovascular Imaging Weill Cornell Medicine and the New York-Presbyterian Hospital, 413 E. 69th Street, Suite 108 New York City, New York, 10021, USA.

E-mail address: sua9028@med.cornell.edu (S.J. Al'Aref).

<https://doi.org/10.1016/j.jcct.2020.01.003>

Received 6 January 2020; Accepted 8 January 2020

Available online 15 January 2020

1934-5925/ © 2020 Society of Cardiovascular Computed Tomography. Published by Elsevier Inc. All rights reserved.

Table 1
Number of submissions to the journal of cardiovascular computed tomography.

Year	# of submissions
2015	301
2016	313
2017	358
2018	391
2019	560

on total plaque volume (TPV) and adverse events in patients with and without diabetes.² One-hundred-eight diabetic patients were propensity-matched to 324 non-diabetic patients, with a median follow-up of 5.6 years. Patients were followed for a composite endpoint of all-cause mortality, acute coronary syndrome (ACS), and late revascularization (>90 days). The endpoint occurred in 18 (16.7%) diabetic and 26 (8.0%) non-diabetic individuals (hazard ratio [HR] 2.3, $p = 0.03$). Diabetic patients had a significantly larger TPV than non-diabetic patients (median 55.1 mm³ vs. 24.9 mm³, $p = 0.02$). A TPV threshold below 110.5 mm³ was identified as a good discriminant of favorable prognosis with respect to the composite endpoint, irrespective of diabetic status. However, a TPV of 110.5 mm³ was associated with worse prognosis in the presence of diabetes. This work may present a novel surrogate marker of cardiac risk moving forward especially in diabetic patients who tend to experience high burden of diffuse atherosclerosis. In a second article, Subramanya and colleagues reported on the increased risk conferred by a more androgenic hormone profile, as defined by higher levels of free testosterone and lower levels of sex hormone binding globulin (SHBG) in a cohort of 2,759 post-menopausal women.³ Over a median follow-up of 4.7 years, women with higher free testosterone levels had relatively greater coronary artery calcium (CAC) progression (odds ratio [OR] 1.26, 95% CI 1.01–1.56), whereas higher SHBG was associated with a lower progression risk (OR 0.80, 95% CI 0.64–0.99), even after adjustment for traditional cardiac risk factors such as lipid profile, blood pressure, and diabetes. These findings provide more support for the important role of an androgenic hormone balance in the progression of CAC in post-menopausal women. In the same issue, Lee et al. evaluated the reproducibility and reliability of quantitative analysis of coronary computed tomography angiography (CCTA) for assessment of coronary atherosclerotic plaques in patients who had undergone clinically indicated serial CCTA at an interscan interval of 3 months.⁴ To this end, 95 patients with CCTA performed with same tube voltage, and 24 patients with different tube voltages were included. With the reasonable assumption that there is no meaningful progression of plaque volume within 3 months, there was no statistically significant difference in plaque volume between the two consecutive studies on a per-segment and per-lesion level ($p > 0.05$). More importantly, even when the tube voltage changed between the two studies, lesion length, area and diameter stenosis, and plaque volumes were not different. These results provide evidence for the robustness of CCTA as a reference non-invasive imaging modality for serial quantitative plaque assessment.

In the *March-April* issue, Al'Aref and colleagues analyzed 4,945 CCTA scans to study the effect of non-statin lipid-lowering therapy (NST) from the CONFIRM (Coronary CT Angiography Evaluation For Clinical Outcomes: An International Multicenter) registry, a prospective, international, multicenter registry of 27,125 patients who underwent baseline CCTA assessment between 2005 and 2009.⁵ After multivariate and propensity score adjustment, NST was not associated with plaque composition subtypes: non-calcified plaque (0.07 increase, 95% CI 0.05–0.20, $p = 0.26$), partially calcified plaque (0.10 increase, 95% CI 0.10–0.31, $p = 0.06$), or calcified plaque (0.18 increase, 95% CI -0.10–0.46, $p = 0.21$). These findings further corroborate the clinical observations that NST (with the exception of ezetimibe⁶) has not been

associated with benefit in clinical trials and observational analyses. In the same issue, Károlyi et al. compared quantitative CCTA to standard clinical read to identify patients with heart transplant with progressive coronary wall thickening.⁷ Thirty-five male patients underwent 256-slice CCTA 1 and 2 years after heart transplant to evaluate for cardiac allograft vasculopathy. Overall, quantitative CCTA was able to detect more patients with progressive coronary wall thickening (defined as $\geq 10\%$ increase), compared to those identified by clinical read (11 patients vs. 22 patients, $p = 0.01$). These results suggest that a quantitative approach may better detect early stages of post-transplant cardiac allograft vasculopathy than conventional techniques. Won and colleagues studied the effects of glycemic status and plaque volume change as assessed by CCTA.⁸ Normoglycemic, pre-diabetic (defined as a fasting glucose 100–125 mg/dL or hemoglobin A1c between 5.7 and 6.4%), and diabetic patients from the PARADIGM (Progression of Atherosclerotic Plaque Determined by Computed Tomographic Angiography Imaging) study were included in the analysis. Plaque volume was assessed on baseline CCTA, and plaque volume change assessed on follow-up CCTA (median interscan period of 3.2 years). At baseline, plaque volumes became progressively higher with worsening glycemic control (51.3 \pm 83.3 mm³ for normal vs. 51.0 \pm 84.3 mm³ for pre-diabetic vs. 72.6 \pm 95.0 mm³ for diabetics, $p < 0.001$). The same pattern was present on the follow-up exam (normal: 51.3 \pm 83.3 mm³, pre-diabetic: 51.0 \pm 84.3 mm³ vs. diabetic 72.6 \pm 84.3 mm³, $p = 0.001$). However, there were no significant differences in the adjusted OR for plaque progression (OR 1.34, 95% CI 0.97–1.853, $p = 0.079$). These findings highlight the importance of glycemic control on atherosclerotic plaque burden, with the lack of an association between glycemic control and plaque progression likely a result of the short follow-up period as well as the risk profile of the studied cohort.⁹ Masuda and others used machine learning (ML) to see if CCTA histogram analysis was able to distinguish atherosclerotic plaque composition when validated against intravascular ultrasound (IVUS).¹⁰ Seventy-eight patients with 78 plaques were examined with CCTA as well as with an integrated back-scatter IVUS system. The 7 histogram parameters that were used to train an XGBoost ML algorithm included minimum and mean values, standard deviation, maximum value, skewness, kurtosis and entropy. The ability of the ML algorithm to distinguish between fibrous-, fatty- and fibrofatty plaques was compared to that of conventional Hounsfield units (HU) thresholds. The ML algorithm yielded a significantly higher area under the receiver-operating characteristics curve (AUC) compared to that of the conventional method (AUC 0.92, 95% CI 0.76–0.92 vs. AUC 0.83, 95% CI 0.75–0.92, $p = 0.001$).

In the *May-June* issue, Dudum and colleagues examined the prognostic significance of CAC scoring in a sub-population within the CAC Consortium with a family history of CAD but at low risk of atherosclerotic cardiovascular disease (ASCVD), defined as <5% 10-year risk.¹¹ A total of 14,169 patients who were followed for an average of 11.6 \pm 2.7 years were included in the analysis. Approximately 11% had a CAC score >100. The absolute event rate in this study was 1.2 (95% CI 1.1–1.4) per 1000 patient-years for all-cause mortality, 0.3 (95% CI 0.2–0.4) per 1000 patient-years for CVD-specific mortality, and 0.2 (95% CI 0.13–0.26) per 1000 patient-years for coronary heart disease (CHD)-specific mortality. Those with CAC score >100 had a 3.0 times higher event rate of all-cause mortality, a 4.7 times higher event rate for CVD-specific mortality, and an 11.4 times higher event rate of CHD-specific mortality. This study confirms the benefits of CAC scoring in patients with a low ASCVD score and a family history of CHD in accordance with the 2018 American College of Cardiology/American Heart Association guidelines.¹² Also in this issue Feuchtnner et al. evaluated the relationship between the amount of exercise and the extent of atherosclerotic plaque, as evaluated by CCTA.¹³ Patient exercise categories were separated into none, low (1–2 times a week), moderate (3–5 times a week), or high (5–7 times a week) as well as total time spent exercising during the week as low (<30 min), moderate

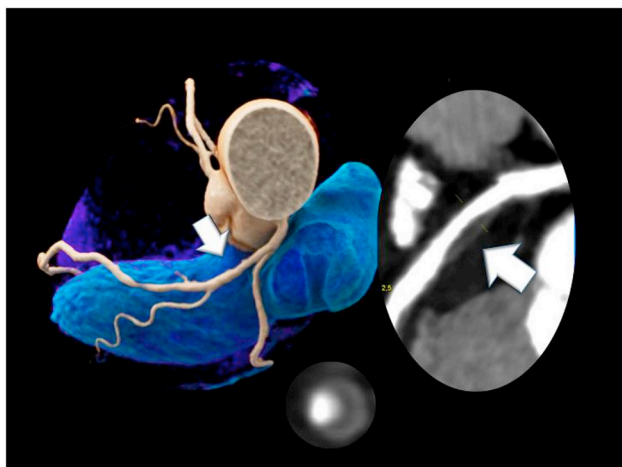


Fig. 1. Curved multiplanar reformation of a 67 year-old-man, inactive, BMI of 27, 2 risk factors, atypical chest pain, CAC score 0, segment involvement score 2, and G-score 8. CCTA (right inset): Non-calcified plaque in the proximal LAD with 3 high-risk criteria (low-attenuation fibrofatty plaque with lipid-necrotic core plaque (4 HU), napkin-ring sign (lower inset), and positive remodeling with a RI 1.5). BMI, body mass index; CAC, coronary artery calcium; CCTA, coronary computed tomography angiography; HRP, high-risk plaque; HU, Hounsfield units; LAD, left anterior descending; RI, remodeling index.¹³

(1 h) or high (>1–3 h). In the 252 included patients, subclinical CAD (any plaque, but no prior history of CAD) was seen in 57.4%. Stenosis severity was lower in the moderate-to-high exercisers as compared to that of inactive patients and low exercisers ($p = 0.008$), and the trend was maintained when comparing the moderate-to-high exercisers with the inactive group alone (Fig. 1). Total and non-calcified plaque burden (as determined by segment involvement score, and non-calcified plaque score G-score) as well as high-risk plaque was less prevalent in the moderate-to-high exercisers. Interestingly, this group of patients also demonstrated a higher CAC score in patients reporting the highest levels of exercise frequency; the bimodal “U-shaped” distribution as previously seen.¹⁴ Despite this distribution, there were no major adverse cardiac events (MACE) seen during the 1 year follow-up period. Clearly the pathways of atherogenesis in recreational athletes are complex and requires further investigation. These results encourage the use of CCTA for the detection of occult CAD in recreational athletes.

In the *July-August* issue, Litwin and colleagues examined how body mass index (BMI) affected the diagnostic yield of CCTA and myocardial perfusion imaging (MPI) among 8,889 patients from the PROMISE (Prospective Multicenter Imaging Study for Evaluation of Chest Pain) trial.¹⁵ A positive CCTA or invasive coronary angiography (ICA) was defined as $\geq 70\%$ stenosis or $\geq 50\%$ if in the left main coronary artery, and a stress test was considered positive in the presence of inducible ischemia. In patients with BMI ≥ 35 vs. < 35 , CCTA positivity was not statistically different (10% vs. 12%), while MPI was more likely to be positive (18% vs. 13%, $p = 0.001$). The likelihood of obstructive CAD at ICA did not differ by BMI category in patients undergoing CCTA (52% vs. 59%), while among MPI patients, ICA was positive in 29% vs. 48%, ($p = 0.005$) with BMI ≥ 35 vs. < 35 , respectively. The authors conclude that the degree of obesity should be considered when choosing evaluation strategies, based on the reduced diagnostic ICA yield of MPI in obese patients. In the same issue, Severance et al. sought to identify the optimal age to screen asymptomatic individuals for CAC, using previously identified risk loci.^{16,17} From 6,660 asymptomatic participants in the MESA (Multi-Ethnic Study of Atherosclerosis), genotype data and CAC scores were obtained and a genetic risk score (GRS) was calculated by summing the number of individual risk alleles multiplied by previously reported ORs. This GRS was found to be predictive of non-zero CAC scores in the entire cohort (multivariate OR 1.37, CI 1.29–1.45), as well as in all individual ethnic sub-cohorts. The genetic

effect was strongest in the youngest cohort (age 44–54, prevalence of non-zero CAC 15.8% for low GRS vs. 31.6% for high GRS). Aiming for a target rate of 25% non-zero CAC scores, the optimal scan age was calculated to be 45.3 years (range, 39.0–51.6) for men, and 55.8 years (range, 49.5–62.1) for women. Similar results were found using a widely available ‘direct-to-consumer’ GRS. The authors concluded that GRS may find utility in not only enhancing the yield of CAC screening, but also in defining an optimal age range in which the probability of non-zero CAC crosses a predetermined threshold. It is worth noting that the study was limited to participants older than 45 of age and yet one quarter of the youngest age group already had clinically detectable calcium. Further research is necessary to validate these results in younger age groups, to understand the age at which calcium becomes clinically detectable.

3. Topic 2: Coronary physiology

In the *January-February* issue, Wardziak and colleagues assessed the diagnostic accuracy of CCTA, CT-fractional flow reserve (FFR_{CT}), and ICA against invasive fractional flow reserve (FFR).¹⁸ Invasive FFR was performed in 96 intermediate stenoses (defined as 50–90% on CCTA) from 90 patients, with 41 of stenoses considered hemodynamically significant. The AUC for determining the functional significance of a coronary lesion was 0.653 for quantitative coronary angiography (QCA), 0.652 for visual ICA, 0.690 for quantitative CCTA and 0.660 for visual CCTA, while the AUC for FFR_{CT} (0.835) was significantly higher compared to the aforementioned assessment methods. FFR_{CT} was performed on a dual-source CT scanner (DECT) (2 x 128; Somatom Definition FLASH, Siemens Medical Solutions, Forchheim, Germany) with dedicated software (cFFR v2.1, Siemens) that utilizes ML algorithms. This work may provide more viable options that will further improve the clinicians’ ability to determine the functional significance of intermediate lesions on CCTA, which has been the Achilles heel of existent technology.

In the *March-April* issue Takagi and colleagues compared 3 different methods of FFR_{CT} interpretation compared to invasive FFR.¹⁹ The 3 methods compared were: (1) change in FFR_{CT} (Δ FFR_{CT}), (2) lesion-specific FFR_{CT}, and (3) lowest FFR_{CT}. Significant obstruction ($\geq 50\%$ diameter stenosis) and ischemia (defined as lesion-specific FFR_{CT} ≤ 0.80 , lowest FFR_{CT} ≤ 0.80 , or Δ FFR_{CT} ≥ 0.12 based on the greatest Youden index) were compared against the reference standard of invasive FFR ≤ 0.80 . Δ FFR_{CT} had the highest AUC (0.86) compared to that of lesion-specific FFR_{CT}, lowest FFR_{CT}, and CCTA (0.71, 0.65 and 0.66, respectively). Moreover, the per-vessel sensitivity and specificity of Δ FFR_{CT} (80%, 95% CI 71–87; 82%, 95% CI 70–90) were comparable to those in the NXT (Analysis of Coronary Blood Flow Using CT Angiography: Next Steps) trial (sensitivity and specificity 84% and 86% respectively).

In the *July-August* issue, van Diemen et al. investigated the relationship between coronary lumen volume to left ventricle mass (V/M) ratio and both non-invasive and invasive reference standards for ischemia.²⁰ The investigators analyzed a total of 152 patients, comprising 431 vessels, who underwent both CCTA and [¹⁵O]-H₂O positron emission tomography (PET) prior to ICA with FFR interrogation of all major epicardial arteries. Coronary plaque analysis and calculation of V/M ratios were semi-automatically performed, and low versus high V/M ratios were classified with respect to the median ratio of the cohort.²¹ Non-invasive ischemia was defined as an impaired hyperemic myocardial blood flow (hMBF) of ≤ 2.30 mL/min/g, while ischemia by FFR was defined as ≤ 0.80 . The investigators found that vessel-specific invasive and non-invasive ischemia was more prevalent in patients with a low V/M ratio as compared to patients with a high V/M ratio. Furthermore, it was demonstrated that V/M ratios were weakly associated with both hMBF and FFR on a per-vessel basis ($r = 0.148$, $p = 0.027$). More interestingly, despite this low association, the V/M ratio remained an independent predictor of FFR ($p = 0.047$) in case of non-obstructive

disease on ICA. These findings suggest that future research is warranted in order to truly elucidate the incremental role of V/M for patients with intermediate lesions that require functional evaluation. Ferencik and colleagues evaluated the performance of FFR_{CT} in identifying ACS, revascularization, and plaque characteristics among patients presenting with acute chest pain and a low-to-intermediate suspicion for ACS.²² Patients from the ROMICAT II (Rule Out Myocardial Infarction/Ischemia Using Computer Assisted Tomography II) study were considered for this analysis. $FFR_{CT} \leq 0.80$ demonstrated a significant association with the presence of high-risk plaque, independent of stenosis severity. The associated relative risk of ACS and revascularization using this cutoff was 4.03 (95% CI 1.56–10.36) and 3.50 (95% CI 1.12–10.96) respectively. These findings support the potential application of FFR_{CT} in the setting of acute chest pain, but requires further investigation with larger and more diverse patient populations. Finally, Hou and colleagues examined the predictive value of obesity defined by BMI or waist-to-height ratio in detecting the presence of plaque or obstructive stenosis in 8,851 consecutive patients with suspected CAD who underwent CCTA.²³ The waist-to-height ratio was calculated as circumference of the waist (cm) divided by height (cm) and was categorized as follows: normal (< 0.5), overweight 0.5 to 0.55, obese, (> 0.55). The AUCs of the waist-to-height ratio for any plaque or obstructive stenosis were 0.561 (95% CI 0.548–0.573) and 0.544 (95% CI 0.529–0.559), respectively, while the AUCs of BMI were 0.513 (95% CI 0.501–0.526, $p = 0.031$), and 0.505 (95% CI 0.491–0.520, $p = 0.483$). Overall, the AUCs for BMI-based predictions were significantly lower than that derived from waist-to-height ratio ($p < 0.001$). These findings provide evidence for the strong consideration of waist-to-height ratio over BMI as they relate to CAD.

4. Topic 3: Structural heart disease

As transcatheter aortic valve replacement (TAVR) procedures continue to increase, so too has the volume of pre-TAVR CT. In order to keep pace with the growing demands in the periprocedural period, a new expert consensus document was released regarding CT imaging in the context of TAVR.²⁴ The 2019 update better reflects the expanding body of literature in the planning and post-procedural assessment, including a grading schematic for annular/sub-annular left ventricular outflow tract calcification, an evolving spectrum of bicuspid aortic valve morphology (Fig. 2), recommendations on identifying the annular plane in Sievers Type 0 morphology, semi-quantitative grading of hypo-attenuated leaflet thickening (Fig. 3), and assessment of coronary obstruction risk in valve-in-valve procedures. This timely update is consistent with efforts across the broader context of multiple professional societies using multiple imaging modalities to better consider the heart.²⁵

In the *January-February* issue, Hosny and colleagues presented an open-source workflow that incorporates 3D printing into benchtop TAVR sizing process in 30 consecutive patients.²⁶ Benchtop sizing was performed on a patient-specific 3D-printed aortic valve apparatus with sizing balloons. Benchtop-predicted “best fit” valve size showed a statistically significant correlation with gold-standard CT measurements of the average annulus diameter ($p < 0.0001$). Quantitative pressure maps were made using a balloon-mounted pressure-indicating film deployed within the 3D model. This pressure impression corresponded to post-TAVR paravalvular leak as documented by post-TAVR trans-thoracic echocardiography (TTE) (Fig. 4). Taken as a whole, future heart teams may consider such a workflow as 3D printing becomes more widespread. In a second publication, Obaid and colleagues used the Philips HeartNavigator III (Philips Healthcare, Netherlands), a commercially available medical imaging software that also allows virtual planning to safely implant a Portico transcatheter heart valve (Abbot Vascular, Illinois, USA) around a Starr-Edwards ball-cage mitral prosthesis.²⁷ Finally Li et al. compared the imaging features of coronary artery-to-pulmonary artery fistulas on CCTA to TTE and ICA.²⁸ Out of a

consecutive series of 19,855 CCTA performed with 256-slice multi-detector row CT (MDCT), 72 patients with coronary artery-to-pulmonary artery fistulas were identified. Of these 72 patients, 47 also underwent TTE and 25 had ICA data. The authors showed that CCTA was able to detect the presence of, origin, number, size, course (tubular, worm-like dilation, significant aneurysm, wall-attachment sign) of fistula vessels, drainage site, drainage site features, and main pulmonary artery enlargement). It is worth pointing out that CCTA is an excellent imaging modality which provides a wealth of information to track this rare condition over time and can potentially guide timing of surgical intervention.

The *March-April* issue highlighted the work of Eberhard and colleagues in their comparison of aortic valve calcification (AVC) scoring performed with software across 4 vendors: syngo.via Calcium Scoring (Siemens Healthineers, Erlangen, Germany), Heartbeat-CS, Intellispace 8.0 (Philips healthcare Eindhoven, The Netherlands), SmartScore 4.0, Advantage Workstation platform Volume Share 7 (GE healthcare, Waukesha, Wisconsin, USA), and 3mensio (Pie Medical Imaging, Maastricht, The Netherlands).²⁹ Two observers performed AVC scoring on 100 patients each across all 4 vendor software with excellent correlation across the vendors (Spearman $r = 0.991$ – 0.996 and $r^2 = 0.981$ – 0.992), with minimal variation in absolute AVC Agatston scores ($p = 0.96$ – 0.98). More importantly, the scoring results did not show a significant difference in likelihood assignment of aortic valve stenosis severity. This work is encouraging for structural heart teams looking to risk stratify their aortic stenosis patients by AVC.³⁰ Kocyigit et al. studied patients with a history of atrial fibrillation (AF) referred for cryoablation and the association with left atrial appendage (LAA) shapes with outcomes.³¹ The 4 morphological subtypes evaluated were the ones described by Kimura et al. (cauliflower, cactus, chicken wing, windsock) in addition to more traditional measurements such as long- and short-axis dimensions.³² The authors found that the non-chicken wing LAA morphology was more prevalent in patients with AF ($p < 0.001$). AF patients also had deeper ($p < 0.001$) and wider ($p < 0.001$) LAA dimensions compared to matched controls in sinus rhythm. At a median follow-up of 37 months, only longitudinal-axis diameter ($p = 0.003$) and cauliflower LAA morphology ($p = 0.004$) were independent predictors of AF recurrence. These results provide further food for thought in considering the prognostic implications of LAA morphology.

In the *July-August* issue di Minno and colleagues performed a systematic review and meta-analysis of the available literature to investigate if AVC measured by CT might improve prediction of cardiovascular risk.³³ Thirteen studies were included incorporating a total of 3,782 patients with calcification of the aortic valve and 32,890 controls. First, they observed an association between AVC and coronary artery calcification (OR 3.8, 95% CI 2.4–6.0, $p < 0.001$). Second, they observed that patients with AVC were at a higher risk for CAD compared to controls (OR 1.7, 95% CI 1.04–2.87, $p = 0.04$) and that AVC was also able to predict overall mortality (AUC 0.90 \pm 0.07).

5. Topic 4: Non-cardiac assessment on CT

In the *January-February* issue, Hammer and colleagues presented their work on vascular access complication prediction during TAVR using 3D CTA-based iliofemoral artery lumen volume (IFV).³⁴ Forty-five patients with vascular access complications were matched for age, sex, peripheral vascular disease, closure device, device size and procedure year. The median IFV for patients with vascular complications was lower than that for those without complications (7.1 ml vs. 10.1 ml, $p < 0.001$). More importantly, IFV had the most favorable AUC for prediction of vascular complications when compared to other ways of assessing the femoral vasculature (i.e. minimal diameter, area or sheath-femoral artery ratio) with an AUC of 0.78. Minimizing vascular access complications is a persistent worry of heart teams, and this study provides a novel measure that can potentially minimize post-TAVR vascular complications.

Classification	Characteristics	Double oblique transverse MPR	Volume rendered en face view systole	Volume rendered en face view diastole
Sievers Type 0/ bicommissural non-raphe type	<ul style="list-style-type: none"> Two fairly symmetric cusps and two commissures Each cusp has one most basal insertion point; thus there is a total of two most basal insertion points 			
Sievers Type 1/ bicommissural raphe type	<ul style="list-style-type: none"> Two of three cusps are conjoined by a raphe Asymmetric cusp sizes with the cusp opposing the raphe (i.e. cusp not participating in raphe formation) being larger than in a tricuspid aortic valve Raphe does not extend to the level of the STJ which is the distinguishing characteristics to a non-opening commissure Size of raphe and degree of calcification can vary <p><i>Upper row: non-calcified raphe</i> <i>Middle row: Moderately calcified raphe</i> <i>Lower row: Severely calcified raphe</i></p>			
Acquired/ functional bicuspid valve (underlying tricuspid anatomy)	<ul style="list-style-type: none"> Underlying tricuspid anatomy with symmetric Sinus of Valsalva Non-opening commissure due to degenerative changes (here RL commissure) Non-opening commissure reaches STJ, which is the distinguishing factor compared to a raphe 			

Fig. 2. The spectrum of bicuspid aortic valve morphology.²⁴

In the *March-April* issue, Matsumoto et al. analyzed the anatomical features of pulmonary veins based on CCT among patients with incomplete cryoballoon ablation for AF.³⁵ The study included 100 patients with CCT referred for AF cryoballoon ablation and measured the entry angle, short- and long-axis length, area and ovality of the 4 major pulmonary vein ostia on CT images. The rate of incomplete ablation was significantly higher for right-sided pulmonary veins ($p < 0.001$). The saliency of the right-sided laterality may have been driven by the degree of angularity of the pulmonary vein entry into the LA. The adjusted OR for incomplete ablation at the right-inferior PV was 1.17 (95% CI 1.09–1.27, $p < 0.001$), whereas the adjusted OR for the right superior pulmonary vein was 1.12 (95% CI 1.01–1.23, $p = 0.014$). Receiver-operating characteristics analysis demonstrated that the optimal cutoff thresholds for the right inferior and superior pulmonary

vein angle to delineate an incomplete ablation were 40.1° and 79.7°, respectively. Overall, the results may help electrophysiologists better formulate an ablation strategy for patients suffering from AF (Fig. 5).

6. Topic 5: Technical aspects of CCT

In the *January-February* issue, Tomizawa et al. published their work on dynamic myocardial computed tomography perfusion (CTP) as performed by single-source 64-row CT.³⁶ 165 patients underwent adenosine-stress dynamic CTP exams on 64-row CT and the myocardial blood flow (MBF) was calculated using the deconvolution technique. The quantitative perfusion ratio was defined as the MBF of myocardium supplied by significantly stenotic epicardial vessels divided by the MBF without such stenosis or infarct. The authors found that the MBF was

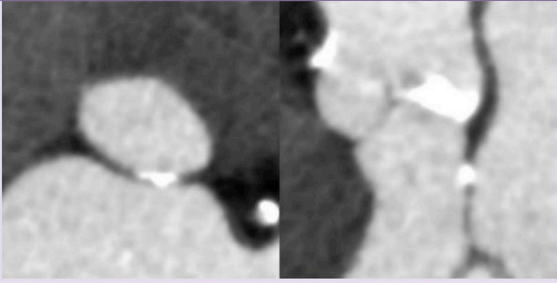
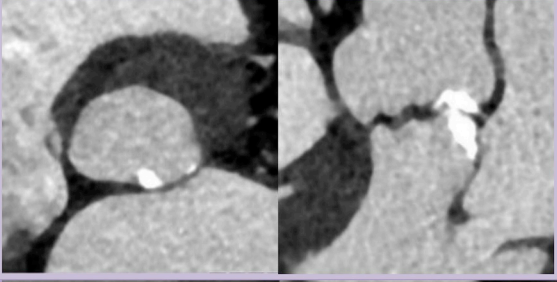
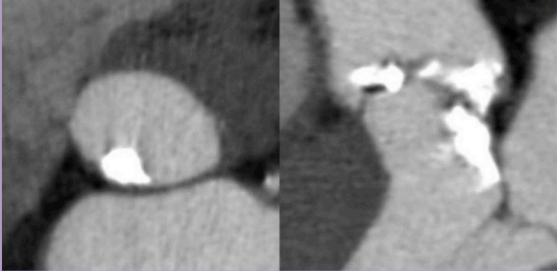
Grade		Examples (
Mild	Single, adherent, non-protruding focus of calcification	
Moderate	Two or more nodules of calcification or a single nodule with limited protrusion into the annular/subannular lumen	
Severe	Single or multiple nodules of calcification, protruding into the annular lumen, and/or extending into the LVOT.	

Fig. 3. Examples of hypo-attenuated leaflet thickening in both self-expandable (upper row) and balloon-expandable device (lower row) with varying degree of thickening: Limited to base, i.e. <25% leaflet involvement (left column) and near complete leaflet involvement, i.e. > 75% (right column).²⁴

1.20 ± 0.32 ml/min/g in myocardium without significant stenosis, which decreased to 0.98 ± 0.24 ml/min/g (p < 0.01) in corresponding myocardium with an associated ≥50% stenosis by QCA. The quantitative perfusion ratio of myocardium subtended by coronary segments with ≥50% by QCA was 0.84 ± 0.32 (95% CI 0.77–0.90, p < 0.001). The accuracy in detecting a QCA- ≥50% stenosis was 82% (95% CI 0.74–0.88) with CCTA alone and 87% (95% CI, 0.80–0.92, p < 0.05) when quantitative perfusion ratio is included. This was all achieved with a radiation dose of 2.5 ± 0.7 mSv with dynamic CTP and 7.3 ± 1.8 mSv for the entire scan. The CTP radiation dose of about 2.5 mSv is notably smaller than previously described doses of 9.23 mSv.³⁷

In the *March-April* issue, Liu et al. considered the feasibility of free-breathing CCTA with a 16-cm z-coverage scan protocol with motion correction.³⁸ Of the 616 patients undergoing CCTA, 325 were performed with breath-hold, and 291 were performed with free-breathing. Image quality score, diagnostic accuracy as compared to ICA, signal-to-noise ratio, and effective radiation dose were compared between the two groups. Notably, there were no significant differences in signal-to-noise ratio and image quality score (p = 0.65). Effective radiation dose also did not differ between the two groups. More importantly, when the sensitivity, specificity and diagnostic accuracy on a per-vessel level were considered, the results were nearly identical. The results may help further extend the utility of CCTA for patients with respiratory concerns previously excluded from such a non-invasive imaging study. Fukui and colleagues assessed the feasibility of a novel feature-tracking CCTA-derived method of assessing global longitudinal strain (GLS) in patients with severe aortic stenosis referred for TAVR.³⁹ A total of 123 consecutive patients with CCTA with a mean left ventricular ejection

fraction (LVEF) of 53 ± 14% were included for analysis with 2D CT-Cardiac Performance Analysis prototype software (TomTec). The calculated GLS demonstrated moderate correlation to that derived by TTE (r = 0.62, p < 0.001), albeit with variability between imaging methods (Fig. 6). GLS assessment continues to gain interest in the community, and its application to CCTA could improve the understanding of ventricular function and dysfunction in structural heart disease.

In the *May-June* issue, Ho and colleagues presented a 2-year single center experience with a clinical CTP service including a real-world referral pattern, technical issues associated in the delivery of care within this program, and the ensuing ICA referrals with outcomes.⁴⁰ The combined mean radiation dose for both rest and stress perfusion was 7.8 ± 3.2 mSv. The mean radiation dose for CCTA was 2.3 ± 1.0 mSv. A total of 123 patients were referred to the CTP service. There were 84 patients who had CAD, with median calcium scores of 357 ± 120, a history of prior percutaneous coronary intervention (PCI) or CAD. After CAC scoring and CCTA, 115 patients had a suitable Coronary Artery Disease Reporting and Data System (CAD-RADS) classification (between 3 and 5) who had stress and rest CTP performed. There were 43 patients with abnormal perfusion, 14 with fixed defects for whom none underwent PCI, and 29 with reversible defects, 18 of whom received PCI, and 11 who were treated medically. All patients who underwent intervention were free from myocardial infarction (MI) or cardiac death, and 88% remained free from MI, death or readmission during a mean follow-up period of 14 ± 8 months. Those with fixed defects or normal perfusion scans were free from MI or cardiac death. Of the 11 patients who were medically managed, 2 underwent PCI for worsening symptoms within 3 months. One patient who had normal perfusion or a fixed defect had angioplasty. Overall, the presented

	aortic root models with deployed sizers		pressure mapping data raw (top) thresholded (bottom)
	photographic	radiographic	
A (23mm)			
B (23mm)			
C (26mm)			
D (29mm)			
E (26mm)			

Fig. 4. Pre-procedural fit-testing of TAVR valves using parametric modeling and 3D printing. Examples of cases without (A and B) and with (C, D, and E) paravalvular leaks. Clock-face positions are used to reference the leak location. Red marking along the hour positions demonstrate confirmed locations of paravalvular leaks, as assessed on post-procedure TTE. Red arrows on the radiographic images depict leak locations qualitatively predicted during experiments. Dashed red lines on the pressure maps demarcate areas of low or no contact pressure that persist from the top edge of the valve (forming a channel); these are areas where leaks were quantitatively predicted. TAVR, transcatheter aortic valve replacement; TTE, transthoracic echocardiography.²⁶ (For interpretation of the references to color in this figure legend, the reader is referred to the Web version of this article.)

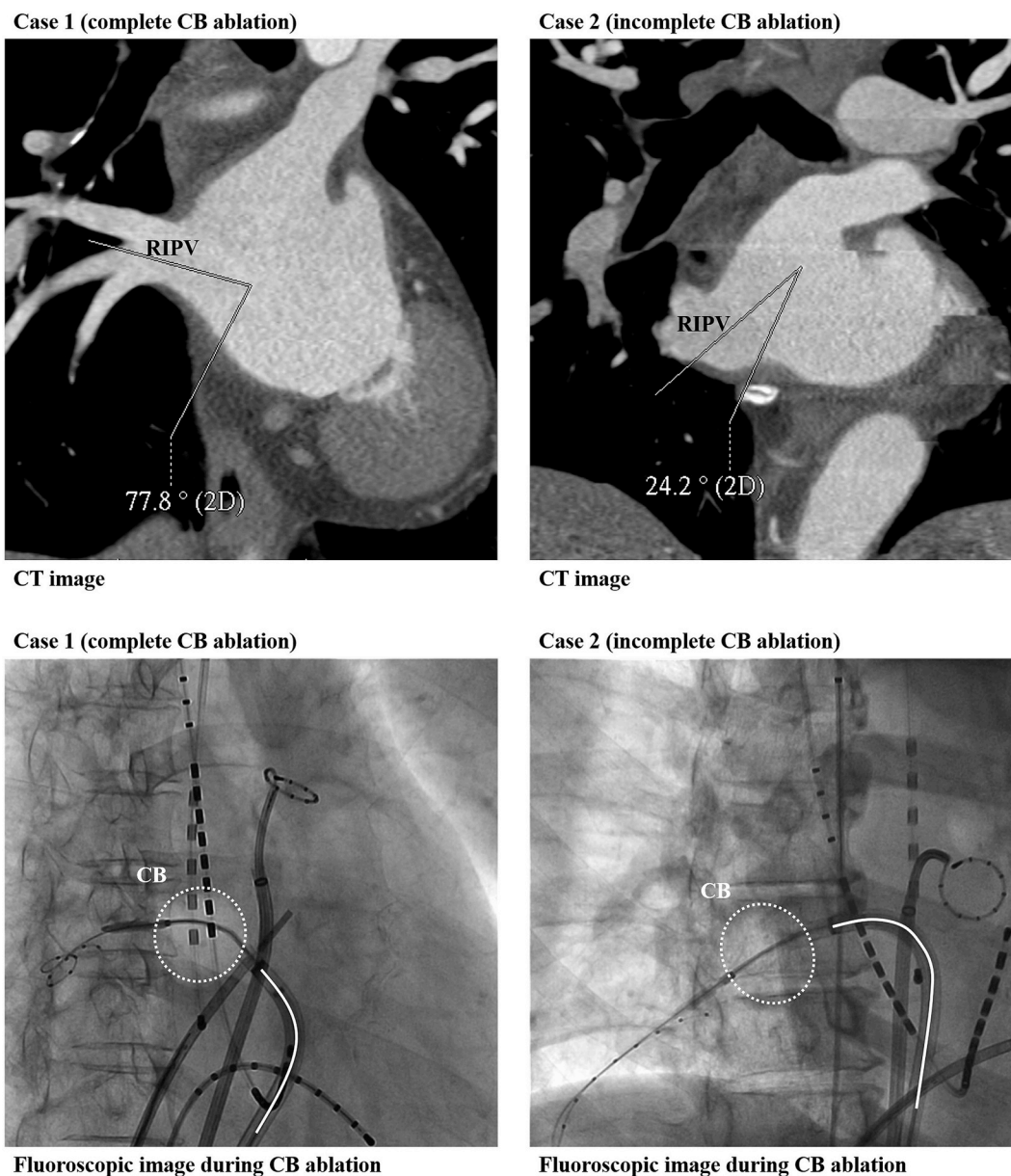


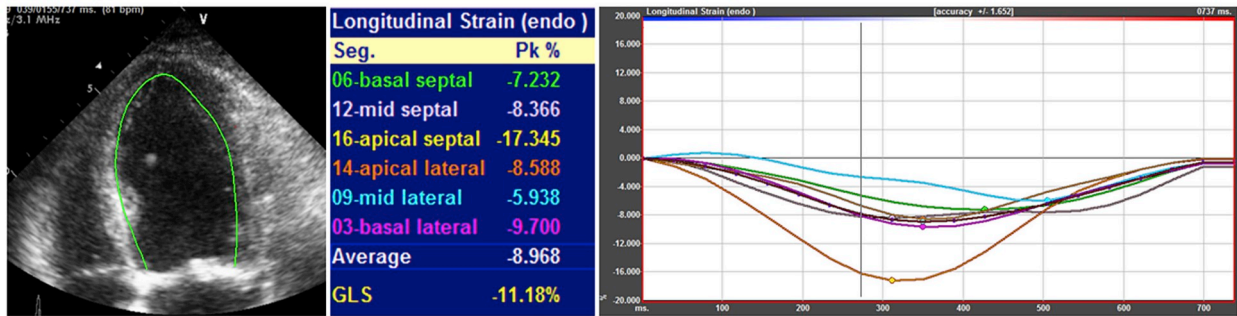
Fig. 5. Representative cases of complete (case 1) and incomplete (case 2) CB ablation. (A, B) MPR images derived from CT images. The RIPV angle was 77.8° in case 1 (A) and 24.2° in case 2 (B). (C, D) Fluoroscopic images (30° RAO view) obtained during CB ablation of the RIPV. On the fluoroscopic image of case 1 (C), the catheter forms a gentle curve. Complete PV isolation was obtained due to good adhesion between the CB and the RIPV ostium and CB ablation was successful. In case 2 (D), the catheter curve was steep and adhesion between the CB and RIPV ostium was inadequate. CB ablation was incomplete. CB, cryoballoon, MPR; multiplanar reconstruction.³⁵

experience demonstrates the utility of CTP as a gate-keeper for ICA with good downstream clinical outcomes. In the same issue, van Assen and colleagues analyzed the prognostic value of CTP and FFR_{CT} with regards to MACE defined as cardiac death, non-fatal MI, unstable angina requiring hospitalization, or revascularization.⁴¹ A total of 243 vessels in 81 patients from 4 institutions underwent dynamic CTP and FFR_{CT} . Twenty-five (31%) patients experienced MACE during a follow-up period of 18 months. In univariate analysis, the index-MBF from the CTP study portion resulted in the largest risk for MACE (HR 11.4) compared to CCTA (HR 2.6) and FFR_{CT} (HR 4.6). Going further, in multivariate analysis that included clinical variables as well as the 3 techniques, only index-MBF significantly contributed to the risk of MACE (HR 10.1), compared to CCTA (HR 1.2) and FFR_{CT} (HR 2.2).

In the *July-August* issue, Matsumoto and colleagues examined the effect of tube potential and luminal contrast attenuation on thresholds for lipid-rich and fibrous plaques on CCTA, as seen on IVUS.⁴² In 52

individuals who underwent kV-adjusted contrast injection protocols, no differences were observed in luminal contrast attenuation, as well as mean attenuation of lipid-rich and fibrous plaque between the kV groups. However, the authors observed that the lumen contrast attenuation increased the attenuation of lipid-rich and fibrous plaque, and that adjusting for lumen attenuation increased the HU differences between the 2 non-calcified plaque types leading to loss of overlap between the plaque types. The authors conclude that plaque attenuation thresholds for non-calcified plaque components should be adjusted based on the luminal contrast attenuation. Liu et al. studied the differences in left ventricular (LV) volume measurements as assessed by attenuation and contour methods.⁴³ The latter traces the LV endothelial border and often includes papillary muscles, generally yielding higher volume measurements than attenuation methods do. On the other hand, attenuation methods utilize a 3D model with thresholding windows, which excludes papillary muscles, and thus may yield smaller volumes

Panel A. GLS in 4 chamber by TTE



Panel B. GLS in 4 chamber by CTA

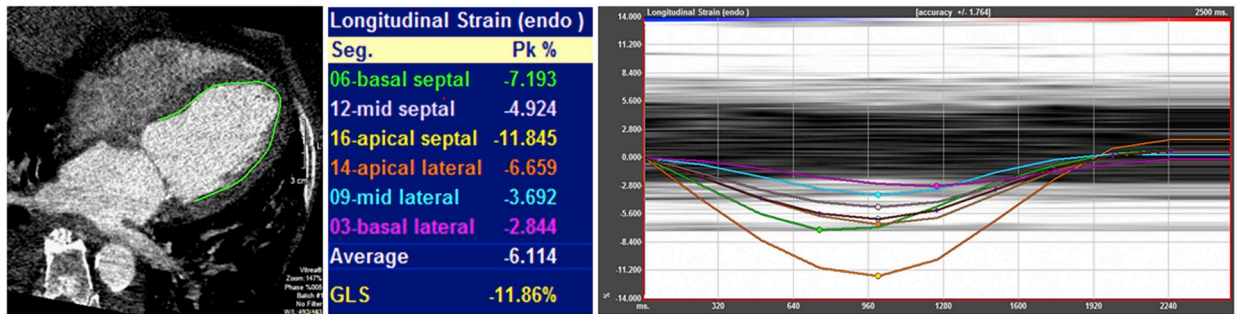


Fig. 6. Panel A – GLS in 4 chamber by TTE. Panel B – GLS in 4 chamber by CTA. CTA, computed tomography angiography; GLS, global longitudinal strain; TTE, transthoracic echocardiography.³⁹

compared to contouring. Among 750 consecutive patients (500 for derivation, 250 for validation cohort) that underwent CCT, LV mid-diastolic volumes (LVMDV) were measured using both methods. In the derivation cohort, (LVMDV_{CON}) volumes measured using contouring was larger than that measured using attenuation (LVMDV_{ATT}) (125.48 ± 46.75 mL vs. 103.06 ± 41.03 mL) with a correlation of r = 0.984. Inter-vendor measurements of LVMDV_{ATT} showed lower variability (103.06 ± 41.03 mL vs. 108.29 ± 44.14 mL; r = 0.969). The derived model was applied to the LVMDV_{CON} in the validation cohort, calculating a corrected LVMDV_{ATT}. Measured and corrected LVMDV_{ATT} measurements did not differ significantly (100.06 ± 48.93 mL vs. 99.80 ± 46.33 mL, p = 0.45). Inter- and intraobserver variability were determined in 50 random patients and were all excellent. This study concludes that careful consideration is required for determining reference values and extrapolating published study results, since LV volume measurements vary by measurement method and vendor. Finally, Nau et al. compared the accuracy of ventricular septal defect (VSD) measurements by high-pitch CT versus that of routine echocardiography and intraoperative findings.⁴⁴ The use of 3D techniques has been found to significantly enhance visualization of septal defects,⁴⁵ which is relevant to patient outcome after surgery.⁴⁶ Additionally, high-pitch dual-source CT minimizes exposure to radiation, which is desirable in young patients.⁴⁷ Fifty-five patients underwent surgical repair of the VSD (median age 8 days, range 1–348 days), as well as pre-operative high-pitch CT and two-dimensional echocardiography. VSD measurements included absolute diameter, normalized area and relative area compared to the aortic valve annulus. Median absolute diameter was similar on CTA and intraoperative findings (12.0 mm vs. 10.8 mm; post-hoc p = 0.09), whereas echocardiographic values were significantly lower (9.6 mm, range 3.0–18.5 mm; both p < 0.01). VSD classifications according to location and orientation matched intraoperative situs in 96.4% using CT and in 87.3% using echocardiography. Pre-operative CT sensitivity and specificity for VSD detection were 97.2% and 98.9%, respectively, compared to echocardiography. Of note, the mean effective radiation dose required was 0.32 mSv (range 0.12–2.0). The authors concluded that in

this pediatric population with congenital heart disease, size and subtype of VSD can be assessed by high-pitch CT with higher accuracy and minimal radiation doses.

7. Topic 6: Technological advances

In the *January-February* issue, van Assen and colleagues presented the feasibility of extracellular volume (ECV) quantification in patients undergoing DECT.⁴⁸ Patients with focal fibrosis, diffuse fibrosis (who also had contrast cardiovascular magnetic resonance studies) and controls underwent non-contrast and delayed acquisitions to calculate single-energy CT (SECT)-ECV. DECT-ECV was calculated from the delayed acquisition scans and virtual non-contrast images. There were no systemic or qualitative differences between the 2 techniques when compared across control, focal fibrosis, and diffuse fibrosis cases, but DECT was able to achieve a radiation saving of 1.1 mSv (p < 0.001). These results may provide an alternative to cardiovascular magnetic resonance-derived ECV in patients with cardiac devices such as pacemakers and defibrillators for example.

The role of CCT quantification of ECV was further explored in the *March-April* issue by Ohta and colleagues evaluated the feasibility of myocardial iodine density and ECV from DECT in identifying non-ischemic dilated cardiomyopathy (NIDCM) from normal hearts.⁴⁹ Thirty-five normal patients and 11 patients with NIDCM were imaged with myocardial delayed enhancement imaging on rapid-kVp switching DECT. Global and segmental iodine density and ECV were calculated from myocardial delayed enhancement images. Global iodine density and ECV were significantly higher in NIDCM compared to normal hearts (14.19 ± 3.90 vs. 10.76 ± 1.88 in 100 µg/cm³, p = 0.015; 31.35 ± 2.53% vs. 26.62 ± 2.69%, p < 0.001, respectively). More importantly, iodine enhancement was able to distinguish between normal myocardium and NIDCM with 91% sensitivity and 60% specificity at a cutoff of 11.18 (AUC 0.812). ECV was able to distinguish between normal hearts and NIDCM with 91% sensitivity and 86% specificity at a cutoff of 28.82 (AUC 0.906). In the same issue, Poulter and colleagues validated a CT-derived MBF and invasive FFR model in a

porcine model. Dynamic CTP and first-pass adenosine stress dual-energy CTP (DE-CTP) was performed in 7 pigs with intracoronary plugs to induce a fixed diameter stenosis.⁵⁰ Quantitative myocardial iodine concentration in first pass DE-CTP was compared to a reference of CT-derived dynamic MBF with normal and compromised blood flow as documented by invasive FFR. FFR best correlated to relative ratios for MBF ($r = 0.86$), myocardial iodine concentration ($r = 0.80$) and CT attenuation number ($r = 0.79$). The correlation between MBF and iodine concentration was modest ($r = 0.42$, $p < 0.003$) but strong between MBF and relative myocardial iodine concentration ($r = 0.88$, $p < 0.0001$). CTP continues to refine itself and the authors have provided useful data to support further investigation of DE-CTP for the evaluation of MBF.

In the *May-June* issue, Annoni and colleagues assessed a low-dose (80 kVp) CCTA protocol for the evaluation of carotid arteries using the latest Iterative Reconstruction (IR) algorithm in comparison to standard 100 kVp scanning with prior generation CT and IR.⁵¹ The scans of 105 patients who were referred for CTA of the carotid arteries with a low-dose protocol were compared to those of 100 patients who were scanned using a conventional protocol. 62 patients in the low-dose protocol group ultimately underwent digital subtraction angiography. Overall, the lower dose protocol demonstrated lower noise, higher signal-to-noise ratio, higher contrast-to-noise ratio compared to the conventional radiation dose scans, and previous generation scanners. Moreover, compared to digital subtraction angiography, the low-dose CTA protocol yielded a sensitivity, specificity, negative predictive value, and accuracy of 100%, 98%, 100%, and 99%. Most importantly, the effective radiation dose in the 80 kV protocol was 0.54 ± 0.1 mSv, in keeping with the aim of low radiation doses for patients.

8. Conclusions

As we look forward to a new year at JCCT, we are first grateful for the editorial staff and the peer reviewers in their assistance in adjudicating the submitted scientific work for consideration of publication. The CT community has benefitted tremendously from the hard work of many, and it is evident that the coming years promise continued refinement and broader innovation made possible many years ago by the recipients of the Nobel Prize in Physiology or Medicine in 1979 Drs. Allan McCormack and Godfrey Newbold Hounsfield.

Sources of funding

No funding was required to support this publication.

Declaration of competing interest

CNC receives research support from and has received speaker fees from Siemens Healthineers. JAL serves as a consultant and holds stock options with Circle CVI and HeartFlow and receives research support from GE Healthcare. JKM receives funding from the Dalio Foundation, NIH, and GE Healthcare. JKM also serves on the scientific advisory board of Arineta and GE Healthcare, and has an equity interest in Cleerly.

Appendix A. Supplementary data

Supplementary data to this article can be found online at <https://doi.org/10.1016/j.jcct.2020.01.003>.

References

1. The Nobel chronicles Raju TN. Allan MacLeod Cormack (b 1924); and Sir Godfrey Newbold Hounsfield (b 1919). *Lancet (London, England)*. 1979;354(9190):1653. [https://doi.org/10.1016/S0140-6736\(05\)77147-6](https://doi.org/10.1016/S0140-6736(05)77147-6) 1999.
2. Deseive S, Straub R, Kupke M, et al. Impact of diabetes on coronary artery plaque

- volume by coronary CT angiography and subsequent adverse cardiac events. *J Cardiovasc Comput Tomogr*. 2019;13(1):31–37. <https://doi.org/10.1016/j.jcct.2018.09.008>.
3. Subramanya V, Zhao D, Ouyang P, et al. Association of endogenous sex hormone levels with coronary artery calcium progression among post-menopausal women in the Multi-Ethnic Study of Atherosclerosis (MESA). *J Cardiovasc Comput Tomogr*. 2019;13(1):41–47. <https://doi.org/10.1016/j.jcct.2018.09.010>.
4. Lee S-E, Park H-B, Xuan D, et al. Consistency of quantitative analysis of coronary computed tomography angiography. *J Cardiovasc Comput Tomogr*. 2019;13(1):48–54. <https://doi.org/10.1016/j.jcct.2018.09.012>.
5. Al'Aref SJ, Su A, Gransar H, et al. A cross-sectional survey of coronary plaque composition in individuals on non-statin lipid lowering drug therapies and undergoing coronary computed tomography angiography. *J Cardiovasc Comput Tomogr*. 2019;13(2):99–104. <https://doi.org/10.1016/j.jcct.2019.01.015>.
6. Cannon CP, Blazing MA, Giugliano RP, et al. Ezetimibe added to statin therapy after acute coronary syndromes. *N Engl J Med*. 2015;372(25):2387–2397. <https://doi.org/10.1056/NEJMoa1410489>.
7. Károlyi M, Kolossváry M, Bartykowszki A, et al. Quantitative CT assessment identifies more heart transplanted patients with progressive coronary wall thickening than standard clinical read. *J Cardiovasc Comput Tomogr*. 2019;13(2):128–133. <https://doi.org/10.1016/j.jcct.2018.11.006>.
8. Won K-B, Lee S-E, Lee BK, et al. Longitudinal assessment of coronary plaque volume change related to glycemic status using serial coronary computed tomography angiography: a PARADIGM (Progression of Atherosclerotic Plaque Determined by Computed Tomographic Angiography Imaging) substudy. *J Cardiovasc Comput Tomogr*. 2019;13(2):142–147. <https://doi.org/10.1016/j.jcct.2018.12.002>.
9. Arnett DK, Blumenthal RS, Albert MA, et al. ACC/AHA guideline on the primary prevention of cardiovascular disease. *J Am Coll Cardiol*. 2019. <https://doi.org/10.1016/j.jacc.2019.03.010> March 2019.
10. Masuda T, Nakaura T, Funama Y, et al. Machine-learning integration of CT histogram analysis to evaluate the composition of atherosclerotic plaques: validation with IB-IVUS. *J Cardiovasc Comput Tomogr*. 2019;13(2):163–169. <https://doi.org/10.1016/j.jcct.2018.10.018>.
11. Dudum R, Dzaye O, Mirbolouk M, et al. Coronary artery calcium scoring in low risk patients with family history of coronary heart disease: validation of the SCCT guideline approach in the coronary artery calcium consortium. *J Cardiovasc Comput Tomogr*. 2019;13(3):21–25. <https://doi.org/10.1016/j.jcct.2019.03.012>.
12. Grundy SM, Stone NJ, Bailey AL, et al. AHA/ACC/AACVPR/AAPA/ABC/ACPM/ADA/AGS/APHA/ASPC/NLA/PCNA guideline on the management of blood cholesterol. *J Am Coll Cardiol*. 2018;73(24):e285–e350. <https://doi.org/10.1016/j.jacc.2018.11.003> 2019.
13. Feuchtnner G, Langer C, Barbieri F, et al. Relationship of exercise to coronary artery disease extent, severity and plaque type: a coronary computed tomography angiography study. *J Cardiovasc Comput Tomogr*. 2019;13(3):34–40. <https://doi.org/10.1016/j.jcct.2019.02.001>.
14. Merghani A, Maestrini V, Rosmini S, et al. Prevalence of subclinical coronary artery disease in masters endurance athletes with a low atherosclerotic risk profile. *Circulation*. 2017;136(2):126–137. <https://doi.org/10.1161/CIRCULATIONAHA.116.026964>.
15. Litwin SE, Coles A, Pagidipati N, et al. Effects of obesity on noninvasive test results in patients with suspected cardiac ischemia: insights from the PROMISE trial. *J Cardiovasc Comput Tomogr*. 2019;13(4):211–218. <https://doi.org/10.1016/j.jcct.2019.03.010>.
16. Severance LM, Contijoch FJ, Carter H, et al. Using a genetic risk score to calculate the optimal age for an individual to undergo coronary artery calcium screening. *J Cardiovasc Comput Tomogr*. 2019;13(4):203–210. <https://doi.org/10.1016/j.jcct.2019.05.005>.
17. van der Harst P, Verweij N. Identification of 64 novel genetic loci provides an expanded view on the genetic architecture of coronary artery disease. *Circ Res*. 2018;122(3):433–443. <https://doi.org/10.1161/CIRCRESAHA.117.312086>.
18. I. Wardziak, Kruk M, Pleban W, et al. Coronary CTA enhanced with CTA based FFR analysis provides higher diagnostic value than invasive coronary angiography in patients with intermediate coronary stenosis. *J Cardiovasc Comput Tomogr*. 2019;13(1):62–67. <https://doi.org/10.1016/j.jcct.2018.10.004>.
19. Takagi H, Ishikawa Y, Orii M, et al. Optimized interpretation of fractional flow reserve derived from computed tomography: comparison of three interpretation methods. *J Cardiovasc Comput Tomogr*. 2019;13(2):134–141. <https://doi.org/10.1016/j.jcct.2018.10.027>.
20. van Diemen PA, Schumacher SP, Bom MJ, et al. The association of coronary lumen volume to left ventricle mass ratio with myocardial blood flow and fractional flow reserve. *J Cardiovasc Comput Tomogr*. 2019;13(4):179–187. <https://doi.org/10.1016/j.jcct.2019.06.016>.
21. Taylor CA, Gaur S, Leipsic J, et al. Effect of the ratio of coronary arterial lumen volume to left ventricle myocardial mass derived from coronary CT angiography on fractional flow reserve. *J Cardiovasc Comput Tomogr*. 2017;11(6):429–436. <https://doi.org/10.1016/j.jcct.2017.08.001>.
22. Ferencik M, Lu MT, Mayrhofer T, et al. Non-invasive fractional flow reserve derived from coronary computed tomography angiography in patients with acute chest pain: subgroup analysis of the ROMICAT II trial. *J Cardiovasc Comput Tomogr*. 2019;13(4):196–202. <https://doi.org/10.1016/j.jcct.2019.05.009>.
23. Hou Z-H, Lu B, Li Z-N, et al. Is waist-to-height ratio better than body mass index as a predictive indicator of coronary atherosclerosis disease? A cohort study. *J Cardiovasc Comput Tomogr*. 2019;13(4):188–189. <https://doi.org/10.1016/j.jcct.2019.06.009>.
24. Blanke P, Weir-McCall JR, Achenbach S, et al. Computed tomography imaging in the context of transcatheter aortic valve implantation (TAVI)/transcatheter aortic valve replacement (TAVR): an expert consensus document of the Society of Cardiovascular

- Computed Tomography. *J Cardiovasc Comput Tomogr.* 2019;13(1):1–20. <https://doi.org/10.1016/j.jcct.2018.11.008>.
25. Doherty JU, Kort S, Mehran R, et al. ACC/AATS/AHA/ASE/ASNC/HRS/SCAI/SCCT/SCMR/STS 2019 appropriate use criteria for multimodality imaging in the assessment of cardiac structure and function in nonvalvular heart disease. *J Am Coll Cardiol.* 2019;73(4):488–516. <https://doi.org/10.1016/j.jacc.2018.10.038>.
 26. Hosny A, Dilley JD, Kelil T, et al. Pre-procedural fit-testing of TAVR valves using parametric modeling and 3D printing. *J Cardiovasc Comput Tomogr.* 2019;13(1):21–30. <https://doi.org/10.1016/j.jcct.2018.09.007>.
 27. Obaid DR, Smith D, Gilbert M, Ashraf S, Chase A. Computer simulated “Virtual TAVR” to guide TAVR in the presence of a previous Starr-Edwards mitral prosthesis. *J Cardiovasc Comput Tomogr.* 2019;13(1):38–40. <https://doi.org/10.1016/J.JCCT.2018.09.009>.
 28. Li J-L, Huang L, Zhu W, et al. The evaluation of coronary artery-to-pulmonary artery fistula in adulthood on 256-slice CT coronary angiography: comparison with coronary catheter angiography and transthoracic echocardiography. *J Cardiovasc Comput Tomogr.* 2019;13(1):75–80. <https://doi.org/10.1016/j.jcct.2018.10.013>.
 29. Eberhard M, Hinzpeter R, Polacin M, et al. Reproducibility of aortic valve calcification scoring with computed tomography - an interplatform analysis. *J Cardiovasc Comput Tomogr.* 2019;13(2):92–98. <https://doi.org/10.1016/j.jcct.2019.01.016>.
 30. Clavel M-A, Messika-Zeitoun D, Pibarot P, et al. The complex nature of discordant severe calcified aortic valve disease grading: new insights from combined Doppler echocardiographic and computed tomographic study. *J Am Coll Cardiol.* 2013;62(24):2329–2338. <https://doi.org/10.1016/J.JACC.2013.08.1621>.
 31. Kocyigit D, Yalcin MU, Gurses KM, et al. Impact of anatomical features of the left atrial appendage on outcomes after cryoablation for atrial fibrillation. *J Cardiovasc Comput Tomogr.* 2019;13(2):105–112. <https://doi.org/10.1016/j.jcct.2019.01.011>.
 32. Kimura T, Takatsuki S, Inagawa K, et al. Anatomical characteristics of the left atrial appendage in cardiogenic stroke with low CHADS2 scores. *Heart Rhythm.* 2013;10(6):921–925. <https://doi.org/10.1016/j.hrthm.2013.01.036>.
 33. Di Minno MND, Poggio P, Conte E, et al. Cardiovascular morbidity and mortality in patients with aortic valve calcification: a systematic review and meta-analysis. *J Cardiovasc Comput Tomogr.* 2019;13(4):190–195. <https://doi.org/10.1016/j.jcct.2019.06.006>.
 34. Hammer Y, Landes U, Zusman O, et al. Iliofemoral artery lumen volume assessment with three dimensional multi-detector computed tomography and vascular complication risk in transfemoral transcatheter aortic valve replacement. *J Cardiovasc Comput Tomogr.* 2019;13(1):68–74. <https://doi.org/10.1016/j.jcct.2018.10.009>.
 35. Matsumoto Y, Muraoka Y, Funama Y, et al. Analysis of the anatomical features of pulmonary veins on pre-procedural cardiac CT images resulting in incomplete cryoballoon ablation for atrial fibrillation. *J Cardiovasc Comput Tomogr.* 2019;13(2):118–127. <https://doi.org/10.1016/j.jcct.2018.11.005>.
 36. Tomizawa N, Chou S, Fujino Y, et al. Feasibility of dynamic myocardial CT perfusion using single-source 64-row CT. *J Cardiovasc Comput Tomogr.* 2019;13(1):55–61. <https://doi.org/10.1016/j.jcct.2018.10.003>.
 37. Danad I, Szymonifka J, Schulman-Marcus J, Min JK. Static and dynamic assessment of myocardial perfusion by computed tomography. *Eur Heart J Cardiovasc Imaging.* 2016;17(8):836–844. <https://doi.org/10.1093/ehjci/jew044>.
 38. Liu Z, Zhang Z, Hong N, et al. Diagnostic performance of free-breathing coronary computed tomography angiography without heart rate control using 16-cm z-coverage CT with motion-correction algorithm. *J Cardiovasc Comput Tomogr.* 2019;13(2):113–117. <https://doi.org/10.1016/j.jcct.2019.01.005>.
 39. Fukui M, Xu J, Abdelkarim I, et al. Global longitudinal strain assessment by computed tomography in severe aortic stenosis patients - feasibility using feature tracking analysis. *J Cardiovasc Comput Tomogr.* 2019;13(2):157–162. <https://doi.org/10.1016/j.jcct.2018.10.020>.
 40. Ho K-T, Ong H-Y, Ong S. Systematic assessment of procedural parameters, influence on downstream testing and 12-month outcomes of a CT-myocardial perfusion service. *J Cardiovasc Comput Tomogr.* 2019;13(3):11–20. <https://doi.org/10.1016/j.jcct.2019.04.006>.
 41. van Assen M, De Cecco CN, Eid M, et al. Prognostic value of CT myocardial perfusion imaging and CT-derived fractional flow reserve for major adverse cardiac events in patients with coronary artery disease. *J Cardiovasc Comput Tomogr.* 2019;13(3):26–33. <https://doi.org/10.1016/j.jcct.2019.02.005>.
 42. Matsumoto H, Watanabe S, Kyo E, et al. Effect of tube potential and luminal contrast attenuation on atherosclerotic plaque attenuation by coronary CT angiography: in vivo comparison with intravascular ultrasound. *J Cardiovasc Comput Tomogr.* 2019;13(4):219–225. <https://doi.org/10.1016/j.jcct.2019.02.004>.
 43. Liu Y, Bourgeois S, Yam Y, Small GR, Chow BJW. Differences in left ventricular measurements: attenuation versus contour based methods. *J Cardiovasc Comput Tomogr.* 2019;13(4):174–178. <https://doi.org/10.1016/j.jcct.2019.08.003>.
 44. Nau D, Wuest W, Rompel O, et al. Evaluation of ventricular septal defects using high pitch computed tomography angiography of the chest in children with complex congenital heart defects below one year of age. *J Cardiovasc Comput Tomogr.* 2019;13(4):226–233. <https://doi.org/10.1016/j.jcct.2019.01.023>.
 45. Chen FL, Hsiung MC, Nanda N, Hsieh KS, Chou MC. Real time three-dimensional echocardiography in assessing ventricular septal defects: an echocardiographic-surgical correlative study. *Echocardiography.* 2006;23(7):562–568. <https://doi.org/10.1111/j.1540-8175.2006.00277.x>.
 46. Sivakumar K, Anil SR, Rao SG, Shivaprakash K, Kumar RK. Closure of muscular ventricular septal defects guided by en face reconstruction and pictorial representation. *Ann Thorac Surg.* 2003;76(1):158–166. [https://doi.org/10.1016/S0003-4975\(03\)00336-9](https://doi.org/10.1016/S0003-4975(03)00336-9).
 47. Ghoshhajra BB, Lee AM, Engel L-C, et al. Radiation dose reduction in pediatric cardiac computed tomography: experience from a tertiary medical center. *Pediatr Cardiol.* 2014;35(1):171–179. <https://doi.org/10.1007/s00246-013-0758-5>.
 48. van Assen M, De Cecco CN, Sahbaee P, et al. Feasibility of extracellular volume quantification using dual-energy CT. *J Cardiovasc Comput Tomogr.* 2019;13(1):81–84. <https://doi.org/10.1016/j.jcct.2018.10.011>.
 49. Ohta Y, Kitao S, Yunaga H, et al. Quantitative evaluation of non-ischemic dilated cardiomyopathy by late iodine enhancement using rapid kV switching dual-energy computed tomography: a feasibility study. *J Cardiovasc Comput Tomogr.* 2019;13(2):148–156. <https://doi.org/10.1016/J.JCCT.2018.10.028>.
 50. Poulter R, Wood DA, Starovoytov A, Smith S, Chitsaz M, Mayo J. Quantified dual energy computed tomography perfusion imaging using myocardial iodine concentration: validation using CT derived myocardial blood flow and invasive fractional flow reserve in a porcine model. *J Cardiovasc Comput Tomogr.* 2019;13(2):86–91. <https://doi.org/10.1016/j.jcct.2019.01.020>.
 51. Annoni AD, Montorsi P, Andreini D, et al. Submillisievert CT angiography for carotid arteries using wide array CT scanner and latest iterative reconstruction algorithm in comparison with previous generations technologies: feasibility and diagnostic accuracy. *J Cardiovasc Comput Tomogr.* 2019;13(3):41–47. <https://doi.org/10.1016/j.jcct.2019.01.009>.